Proceedings of GT2005
ASME Turbo Expo 2005: Power for Land, Sea and Air
June 6-9, 2005, Reno-Tahoe, Nevada, USA

GT2005-68495

THE EFFECT OF WATER VAPOR ON Cr DEPLETION IN ADVANCED RECUPERATOR ALLOYS

Bruce A. Pint
Oak Ridge National Laboratory
Metals and Ceramics Division
Oak Ridge, Tennessee 37831-6156
Phone: (865) 576-2897, E-mail: pintba@ornl.gov

ABSTRACT

Durable alloy foils are needed for gas turbine recuperators operating at 650°-700°C. It has been established that water vapor in the exhaust gas causes more rapid consumption of Cr in austenitic stainless steels leading to a reduction in operating lifetime of these thin-walled components. Laboratory testing at 650°-800°C of commercial and model alloys is being used to develop a better understanding of the long-term rate of Cr consumption in these environments. Results are presented for commercial alloys 709, 120 and 625. After 10,000h exposures at 650° and 700°C in humid air, grain boundary Cr depletion was observed near the surface of all these materials. In the Fe-base alloys, 709 and 120, this depletion led to localized Fe-rich nodule formation. This information then can be used to develop low-cost alternatives to currently available candidate materials.

INTRODUCTION

Improving gas turbine engine efficiency has always been an attractive goal for reducing operating costs and net emissions. However, increasing engine temperatures to increase efficiency often requires more expensive materials to meet durability goals. With rising fuel costs, it is easier to justify the use of such high temperature alloys in a cost benefit analysis.

One example of this type of materials upgrade is for applications in recuperators or heat exchangers used to improve the efficiency of microturbines and small gas turbines[1]. Over the past 10 years, research and development efforts have been directed at finding replacements for type 347 (Fe-18Cr-10Ni) stainless steel, which is the standard material used for recuperators operating to ≈600°C[2]. At higher temperatures, it has been demonstrated that type 347, like similar composition 300-series stainless steels, is susceptible to accelerated oxidation attack (AA) in exhaust gas due to water vapor from the combustion process[3-9]. Clear replacement candidates have been identified. For example, alloy 625 (Ni-22Cr-9Mo) was appropriate for the recuperator in the Solar Turbine Inc. 4.6MW Mercury 50 gas turbine with an overall efficiency of 38.5%[10] and could easily increase recuperator operating temperatures into the 650-700°C range. However, for small (30-250kW) single-shaft, gas turbine engines or microturbines[11], initial cost is a more significant market issue and a Ni-base alloy may be prohibitively expensive. Therefore, some work has focused on Fe-base alloys, such as alloy 709 (Fe-20Cr-25Ni)[12,13] or Fe-20Cr-20Ni, which model alloy work[7-9,14] suggested may provide sufficient oxidation resistance in this environment. The model alloy results also indicated that higher alloyed materials such as alloy 120 (Fe-25Cr-35Ni) should be even more durable.

In order to determine if these candidate alloys have sufficient corrosion resistance to meet the recuperator durability goal of 40,000h set by the U.S. Department of Energy's Distributed Energy Program[15], laboratory testing in a simulated exhaust gas environment is being conducted. One objective is to obtain a clearer mechanistic understanding of the role of water vapor in this environment. Long-term test results are presented, illustrating the effect of water vapor additions and the effect of test temperature on the amount and type of Cr depletion.

EXPERIMENTAL PROCEDURE

The materials tested in this study were a combination of commercial alloys and laboratory-melted model alloys. Some of the materials were obtained from commercial vendors in foil form, while others were obtained in thicker sections and then hot and cold rolled at Oak Ridge National Laboratory (ORNL) to ≈100μm thickness with average grain sizes given in Table I. Model alloys were vacuum induction melted at ORNL and hot and cold rolled to 1.25mm sheet. After the final cold rolling step, the sheets were annealed in Ar for 2min at 1000°C. Selected alloys were then rolled to foil under similar conditions as used for the commercial alloys. The chemical compositions of representative alloys are shown in Table I.

Specimens (≈1 x 12 x 18mm) cut from sheet material were polished to a 600 grit surface finish. Similar-sized foil (≈100μm) specimens were tested in the as-rolled condition. All specimens were

Table I. Alloy chemical compositions (weight %) and average grain sizes (μm) of the foil and sheet materials. (Balance Fe except for 625.)

	Cr	Ni	Mn	Si	Other	Grain Size (μm)
Type 347	17.8	9.9	1.6	0.5	0.5Nb	5
709	20.3	24.7	1.0	0.4	1.5Mo,0.2Nb	16
120	24.7	37.6	0.7	0.2		13,23*
625	23.1	63.8	0.04	0.2	8.9Mo, 4Nb, 3Fe	12
Fe-16/20+2Mn	15.8	19.7	1.7	0.2		26
Fe-20/20+4Mn	20.9	20.8	3.8	0.2	0.3Nb,0.3Cu,0.3Mo	10

* ORNL- and commercial-rolled foils, respectively

cleaned in acetone and methanol prior to oxidation and mass changes were measured using a Mettler-Toledo model AG245 balance. Exposures were 100h cycles at 650°, 700° or 800°C.

Oxidation exposures in humid air were conducted by flowing the gas at 850 cc/min through an alumina tube that was inside a resistively-heated tube furnace. Distilled water was atomized into the flowing gas stream above its condensation temperature and heated to the reaction temperature within the alumina tube. Water was collected and measured after flowing through the tube to calculate its concentration and calibrate the amount of injected water. A water content of 10±1 vol.% was used for these experiments. Up to 40 specimens were positioned in alumina boats in the furnace hot zone so as to expose the specimen faces parallel to the flowing gas. For testing in air, the alumina furnace tubes were not sealed. After oxidation, selected specimens were Cu-plated and sectioned for metallographic analysis and electron probe microanalysis (EPMA) to determine Cr depletion.

RESULTS

Oxidation in Laboratory Air

To give perspective to the importance of added water vapor, Figure 1 shows oxidation results for several stainless steel foils in laboratory air at 650°C. The mass gain is plotted versus the square root of time to show the parabolic relationship [16]. Without the addition of water vapor, specimens of type 347 and alloy 709 formed a protective, slow-growing scale during ≤50,000h tests. A thin Cr- and Mn-rich oxide scale formed in laboratory air without the Fe-rich oxide nodules formed in the presence of water vapor at 650°C (Fig. 2).

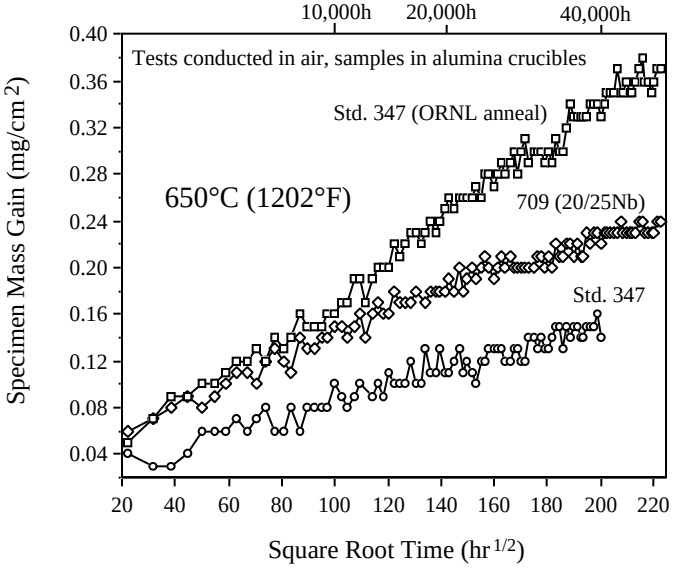

Figure 1. Specimen mass gain of various stainless steels plotted versus square root time to show the parabolic relationship during 500h cycles in laboratory air at 650°C.

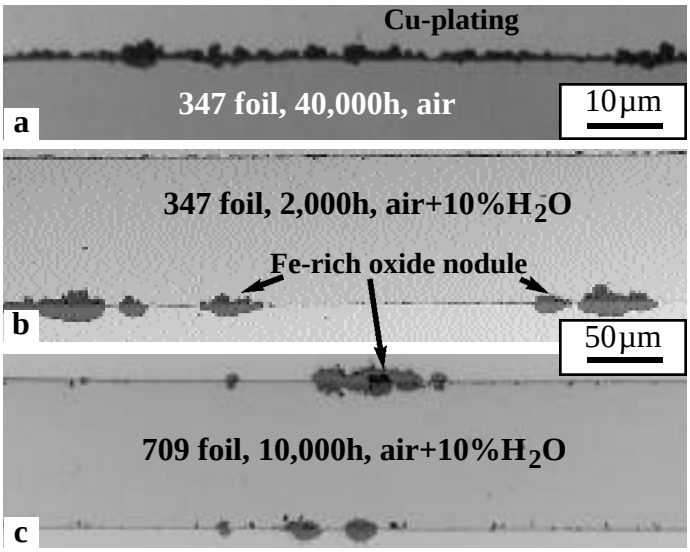

Figure 2. Light microscopy of polished cross-sections of stainless steel foils oxidized at 650°C: (a) type 347, 40,000h in air (b) 347, 2,000h in humid air and (c) alloy 709, 10,000h in humid air.

Oxidation Results at 650°C

Figure 3 shows that the addition of 10% water vapor at 650°C resulted in AA (i.e. high mass gains) for type 347 foils after <2,000 h, when Fe-rich nodules began to form on the specimen surface (Fig. 2b). These nodules grew wider and deeper with time, consuming a large

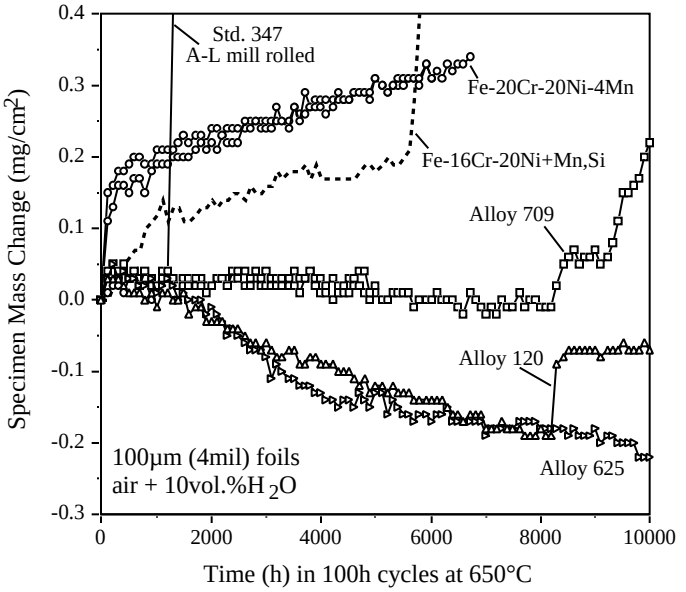

Figure 3. Specimen mass gains for various foil (100μm thick) materials during 100h cycles in humid air at 650°C.

fraction of the foil thickness in relatively short times. The onset of AA was delayed in higher alloyed steels. Figure 3 shows the results for 10,000h (100, 100h cycles) exposures for a number of foil materials. The commercial foils, alloys 120, 625 and 709 initially showed low mass gains or losses. The losses are attributed to the volatilization of $CrO_2(OH)_2$[5]. However, the specimen of Fe-20Cr-25Ni+Nb (rolled from 709 or 20/25Nb) showed increased mass gain (the onset of AA) during the last 2,000h of testing (Figs. 2c and 3). The specimen of alloy 120 (Fe-25Cr-35Ni) also showed an increase at one point but did not continue to gain afterwards. A specimen of Ni-base alloy 625 also showed a fairly continuous mass loss during the test and no indication of AA. Two foil specimens of Fe-20Cr-20Ni-4Mn also were tested at 650°C. This material shows a higher mass gain which is attributed to its high Mn content which increases the Mn content in the scale and its growth rate[14,17].

Oxidation Results at 700°C

Figure 4 shows specimen mass gains for the same materials at 700°C for up to 10,000h. Again, low mass gains or losses indicate protective behavior with a thin oxide and some evaporation. A specimen of alloy 709 stopped after 5,000h showed protective behavior while a second specimen, continued to 10,000h, showed an increase after ≈8,500h. Similar mass change results were found for mill-rolled and ORNL-rolled alloy 120 foils. As at 650°C, the mass gain for Fe-20Cr-20Ni-4Mn was higher than for the other materials, but no nodule formation was observed in a specimen stopped after 6,000h.

Oxidation Results at 800°C

Mass change results at 800°C in humid air are shown in Fig. 5. Only the foil specimen of alloy 120 was run to 10,000h. This specimen showed a larger mass gain for the last 2,000h of the test, suggesting the onset of AA. However, it was a relatively modest increase in mass compared to some of the other specimens. The foil specimen of alloy 625 was stopped at 6,000h for characterization and did not show any signs of AA[7]. Two specimens of alloy 709 were stopped after 6,000

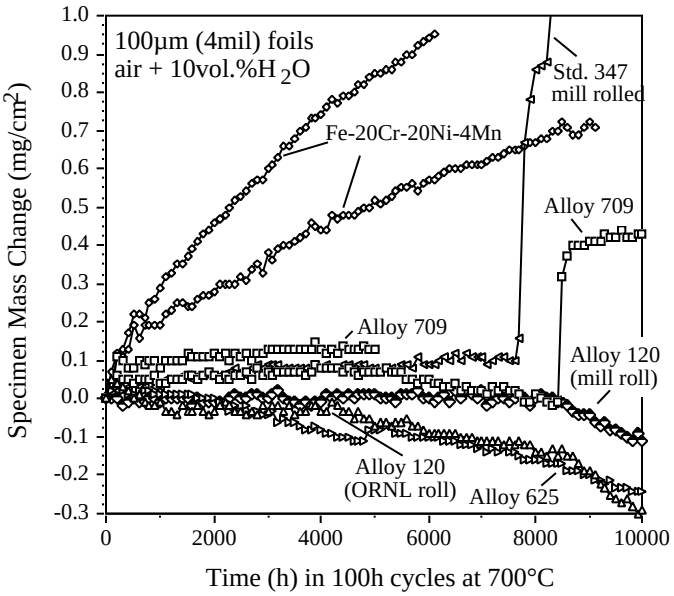

Figure 4. Specimen mass gains for various foil (100µm thick) materials during 100h cycles in humid air at 700°C.

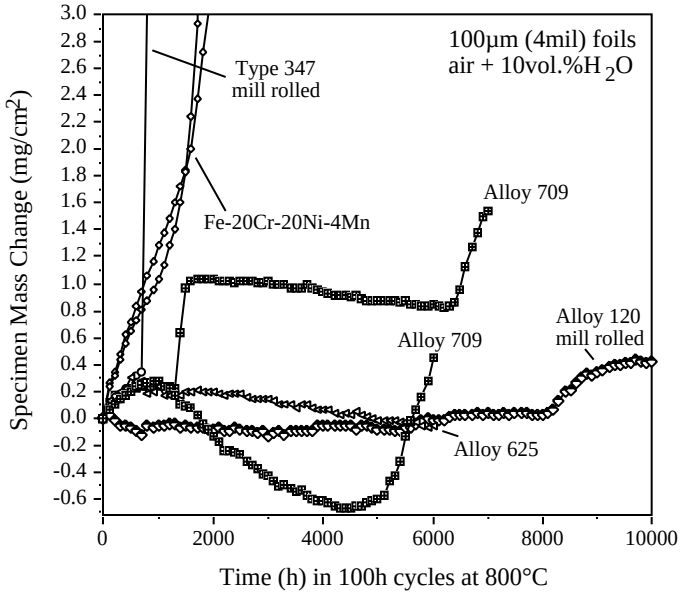

Figure 5. Specimen mass gains for various foil (100µm thick) materials during 100h cycles in humid air at 800°C.

and 7,000h, when rapid mass gains were observed. Two specimens of Fe-20Cr-20Ni-4Mn were stopped after 2,000h due to excessive mass gain. These specimens outlasted commercial 347 foil, which showed AA after less than 1,000h at 800°C (Fig. 5). However, this incremental improvement was likely reduced, due to the higher oxidation rate of this high Mn material. New laboratory scale heats, with compositions based on Fe-20Cr-20Ni, have been fabricated in an attempt to achieve better corrosion resistance.

In general, the failure times for the various foils show the benefit of increasing Cr and Ni contents. Alloy 120, with the highest Cr and Ni contents of the Fe-base alloys, only showed a modest increase in mass after 8,000h. A similar benefit was noted in a series of model alloys containing different Cr and Ni contents (Fig. 6). Sheet specimens were used in this test and all of the alloys contained ≈1.7%Mn and 0.25%Si (e.g. Table I). Unlike foil specimens, the onset of AA for sheet specimens led to scale spallation and a mass loss (likely due to thermal stresses in the oxide). Like the commercial alloy foils, the model alloy results showed that the time to AA increased with increasing Cr and/or Ni contents. The lowest alloyed material, Fe-16Cr-15Ni, showed AAafter the first 100h cycle. The highest alloyed material, Fe-20Cr-25Ni, has yet to show AAafter 4,300h.

Characterization by EPMA

In typical high temperature oxidation experiments conducted in laboratory air, there is some reasonable correlation between mass gain and the thickness of the reaction product. As noted previously[7], this is not the case for testing in humid air due to the significant evaporation. In general, the specimen mass changes ($\Delta M_{specimen}$) from these results are a combination of mass changes from several factors, including oxide growth, evaporation and spallation of the reaction product:

$$\Delta M_{specimen} = \Delta M_{oxide\ growth} - \Delta M_{evap.} - \Delta M_{spall} \quad (1)$$

Thus, while mass gain can be used to differentiate the onset of AAit is

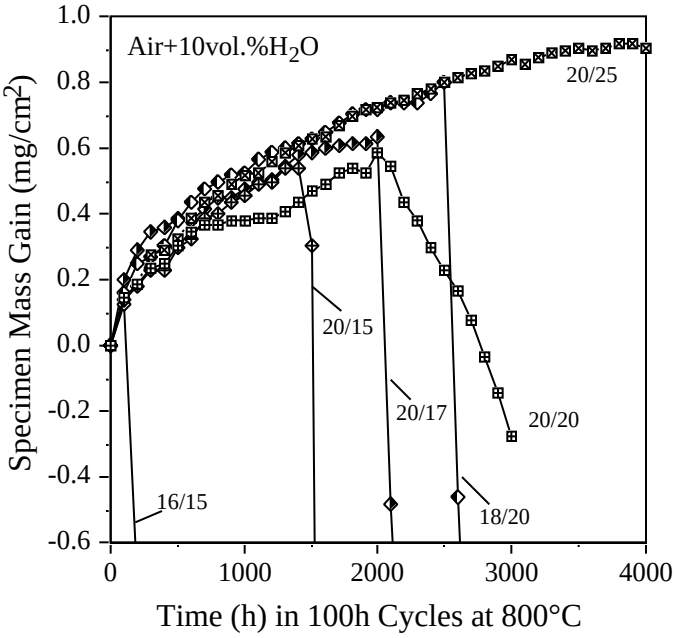

Figure 6. Specimen mass changes for model Fe-Cr-Ni alloys (designated by [Cr]/[Ni]) with Mn and Si additions during 100h cycles in air plus 10%H_2O at 800°C. With increasing Cr and/or Ni contents, time to accelerated attack was increased.

not very useful in quantifying the extent of attack because of these competing processes. Thus, additional characterization of the residual Cr content is necessary.

Figure 7 gives an example of quantitative Cr concentration profiles that were measured across mounted cross-sections of a 100μm thick alloy 120 foil specimen. In general, three profiles with a 1μm

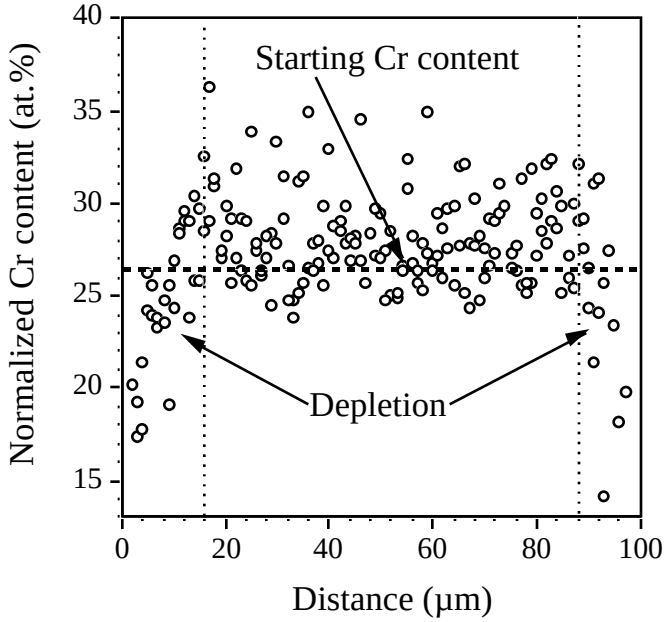

Figure 7. EPMA Cr profiles from two scans across the entire cross-section of 100μm thick alloy 120 foil after 10,000h at 650°C in humid air. The Cr depletion appears to be only 12-15μm from the surface.

Table II. Remaining Cr (% of starting content) and the actual amount of Cr consumed (wt.%) for various foil materials oxidized in humid air for 10,000h (except where noted).*

Alloy	650°C	700°C	800°C
709	92±5% -1.7±1.0wt%	89±4% -2.2±0.8wt%	51±2% (6,000h) -10.2±0.5wt%
120 (ORNL)	94±1% -1.6±0.3wt%	91±2% -2.3±0.6wt%	
120 (Commercial)		92±4% -2.1±0.9wt%	53±1%(10,000h) -11.8±0.5wt%
625	94±4% -1.5±0.9wt%	89±2% -2.6±0.6wt%	77±4% (6,000h) -5.3±0.9wt%

* The standard deviation for three EPMA profiles is indicated.

step size were taken across the foil thickness. A Cr depletion zone was noted at both surfaces. In the center of the specimen, the Cr content was not uniform due to the precipitation of Cr-rich phases in these materials. For the specimens exposed at 650° and 700°C in humid air, the depletion depth was generally 10-20μm with the center of the foil being relatively unchanged. As expected, the depth and amount of depletion increased with increasing time and temperature.

The amount of Cr remaining was determined from the profiles by summing the Cr in each 1μm increment across the foil which also specified the remaining foil thickness. This value was then compared with the starting specimen thickness and Cr content.. Table II summarizes the results for the three commercial alloy foil compositions exposed for 10,000h at 650° and 700°C and various times at 800°C. As expected, the residual Cr dropped with increasing exposure temperature. However, due to the different starting Cr contents (Table I), the percentage values are not directly comparable. The Cr depletion also is presented as the amount of Cr consumed in wt.%. For example, for alloy 625 after 10,000h at 650°C in humid air, ≈6% of the original 23wt.%Cr reservoir was consumed with ≈21.5wt.% Cr remaining, or a loss of ≈1.5wt.%. Comparing these values for the three materials shows that a very similar amount of Cr was consumed in the foils after 10,000h at 650° and 700°C in humid air. A slightly higher amount of Cr consumption was noted for alloy 625 at 700°C, perhaps related to the absence of Mn in this material, which is thought to inhibit Cr evaporation[18]. However, this difference is within the scatter band of the other two materials.

The results are more difficult to compare at 800°C because of the different exposure times. The large amount of Cr consumption for alloy 709 reflects the onset of AAfor this specimen between 5,000 and 6,000h (Fig. 5). A similar loss of Cr for alloy 120 after 10,000h also likely reflects the increased mass gain between 8,000 and 10,000h associated with AA. Alloy 625 showed much less Cr loss after 6,000h and showed no signs of excessive oxidation when the test was stopped. (Fe-rich nodule formation associated with AAwould not occur on a Ni-base alloy.)

In order to better understand the change in Cr content with exposure time, a series of alloy 709 foil specimens was exposed in 1,000h increments at 800°C in humid air. Figure 8 shows the percentage of the Cr remaining from the starting material for specimens exposed in humid air, compared to two specimens exposed in laboratory air. The laboratory air specimens showed a typical parabolic relationship with exposure time for the Cr consumption consistent with

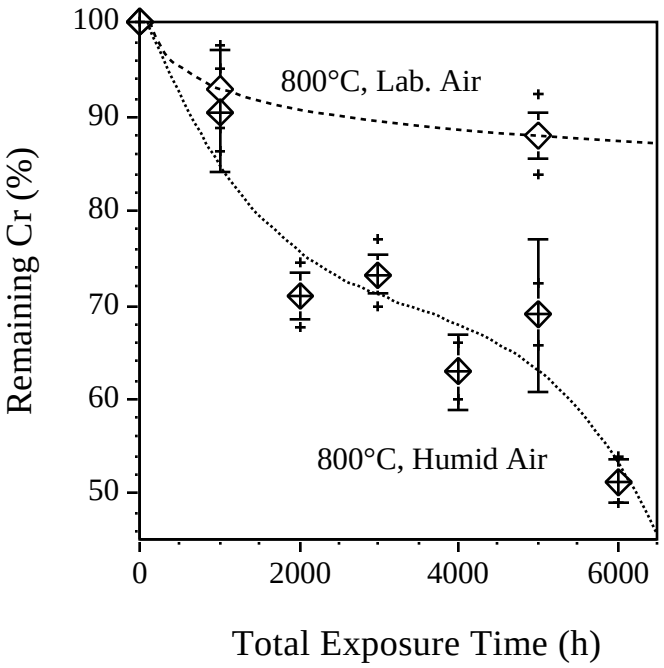

Figure 8. Remaining Cr (% of starting content) measured in alloy 709 specimens exposed for various times at 800°C in humid and laboratory air, assuming a starting Cr content of 21%. Exposures in humid air appeared to increase the rate of Cr depletion. The (+) signs mark the change in calculated Cr if the starting Cr content was 1% higher or lower.

growth of a protective surface oxide layer. After 1,000 h, the humid and laboratory air specimens showed similar Cr consumption. However, at longer times, the specimens exposed in humid air showed increasingly higher Cr losses, with a precipitous drop in residual Cr between 5,000 and 6,000 h, consistent with the mass gain data and the onset of rapid metal consumption during AA. A similar drop in residual Cr likely occurred for alloy 120 after the onset of AAnear 8,000 h.

One of the surprising findings from the 10,000h exposures that was observed in the mass change data (Fig. 3) and confirmed during post-test characterization was the nodule formation observed for alloys 709 (Figure 2c) and 120. Previously, it was assumed that alloys with high Cr and Ni contents (i.e. alloys 120 and 709) would be virtually immune from AA at these temperatures. The reason that these alloys are susceptible to AA is reflected in Fig. 7, where the Cr depletion in alloy 120 was confined to a thin (12-15μm) surface region in the metal. For this narrow region, >25% of the total Cr content had been consumed after 10,000h at 650°C. EPMA maps of the Cr content clearly illustrate the situation (Fig. 9). Not only was the Cr depletion concentrated near the surface, but also the alloy grain boundaries had been selectively depleted. Whenever the localized depletion reached a critical level, ≈10at.% Cr, AA was observed. In these maps, bright areas mark Cr-rich carbides (e.g. M_6C and $M_{23}C_6$[19,20]) phases in the metal and the Cr-rich oxide at the specimen surface. Chromium also was enriched in the large oxidized region that formed into the metal beneath the Fe-rich outer oxide nodules (arrows in Fig. 9). Alloy 625 also showed grain boundary depletion of Cr but, with little Fe present, did not form nodules. Both alloys 709 and 120 were susceptible to AA after 10,000h at 650°C (Figs. 9a and 9c). However, at 700°C, only

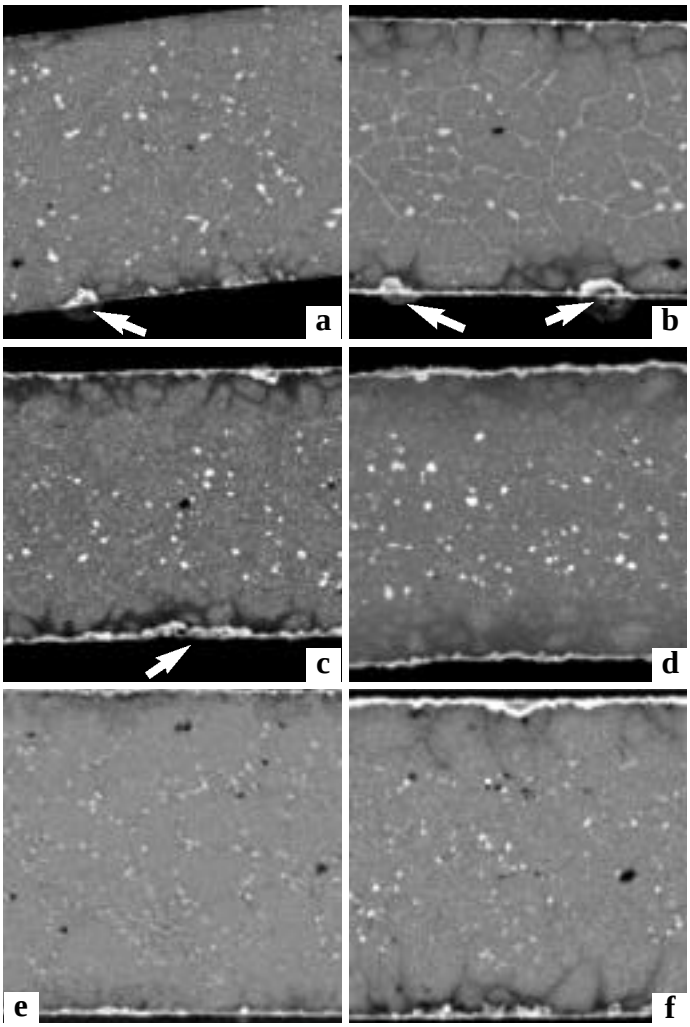

Figure 9. EPMACr maps after 10,000h exposures in humid air of (a) alloy 709 at 650°C, (b) alloy 709 at 700°C, (c) alloy 120 at 650°C, (d) alloy 120 at 700°C, (e) alloy 625 at 650°C and (f) alloy 625 at 700°C. The foils are all 100μm in thickness and arrows mark nodule formation.

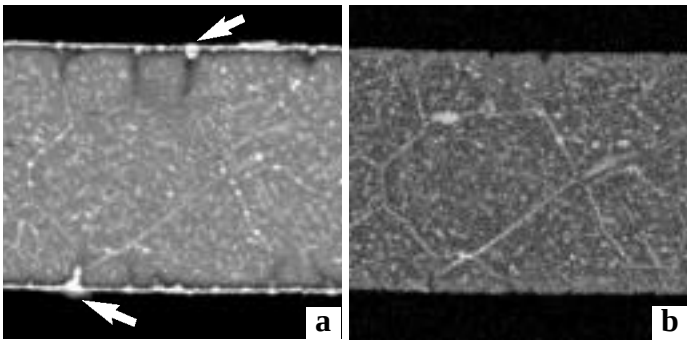

Figure 10. EPMAmaps of 90μm thick commercial alloy 120 foil after a 10,000h exposure in humid air at 700°C (a) Cr, and (b) Mo. A grain-boundary phase containing Cr, Mo and Si marked the large grains within the metal and Cr depletion was observed on grain boundaries near the surface.

alloy 709 formed nodules after 10,000h as a result of Cr-depletion on the alloy grain boundaries near the surface (Fig. 9b). With its higher Cr and Ni contents, alloy 120 did not appear to show significant depletion or AAafter 10,000h at 700°C (Fig. 9d). This is likely due to faster Cr diffusion at 700°C, which allowed Cr from the center of the specimen to diffuse to the surface and reduce the extent of the depletion.

Commercial and ORNL-rolled alloy 120 specimens were oxidized for 10,000h at 700°C and showed similar mass changes (Fig. 4) and Cr depletion (Table II). However, the commercial material had a significantly larger grain size (23±6μm) compared to the laboratory material (13±3μm). The Cr map for the commercial material is shown in Fig. 10a with several nodules forming at depleted alloy grain boundaries, unlike the finer grained material (Fig. 9d). The coarser grain size may have resulted in more severe Cr depletion on the grain boundaries. Another difference between the two materials was the carbide morphology. Much finer M_6C particles[20] were observed in the commercial material after the 10,000h exposure. A map of the Mo content (Fig. 10b) shows the precipitates, which also contained Cr and Si, highlighting the alloy grain boundaries.

Characterization of some of the model alloys after long exposures in humid air also is continuing in order to better understand the oxidation mechanisms in this environment. Even though these specimens are typically 1.2mm thick, they exhibit similar surface depletion and AA as the foil specimens. For example, Fig. 11 shows results for Fe-16Cr-20Ni-2Mn+Si which began to exhibit mass gain associated with AAafter 5,000h at 650°C in humid air and was stopped after 7,000h (dashed line in Fig. 3). This specimen showed numerous nodules on the surface, the outer portion of which were rich in Fe (arrow in Fig. 11a). The Cr map in Fig. 11b shows Cr depletion in the alloy beneath the nodules and a very strong Cr signal in the oxide beneath each nodule. This suggested that a Cr-rich oxide re-formed and prevented the nodule from growing. A line profile in an area without any overlying nodules showed the Cr content was ≈13wt% (15at.%) in the alloy grain adjacent to the surface and ≈11at,% near a grain boundary (Fig. 12). A line profile beneath an oxide nodule

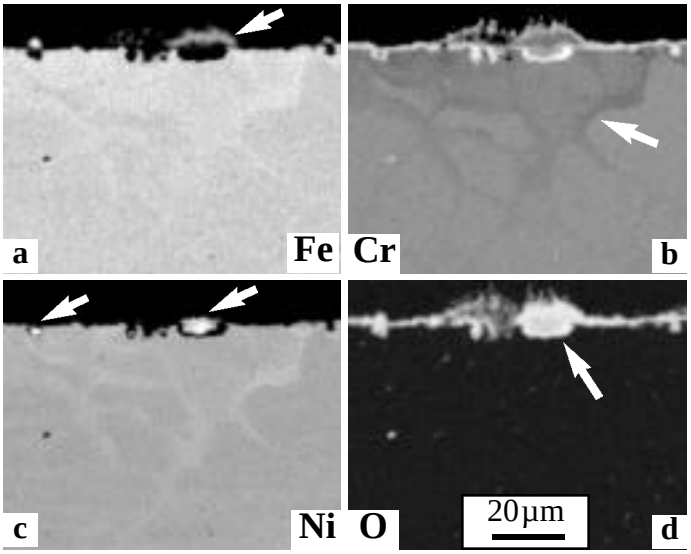

Figure 11. EPMA maps of Fe-16Cr-20Ni-2Mn+Si after 7,000h at 650°C in humid air: (a) Fe, (b) Cr, (c) Ni and (d) O. Surface oxide nodules having a Ni-rich center, a Cr-rich underlayer and a Fe-rich outer layer have begun to form.

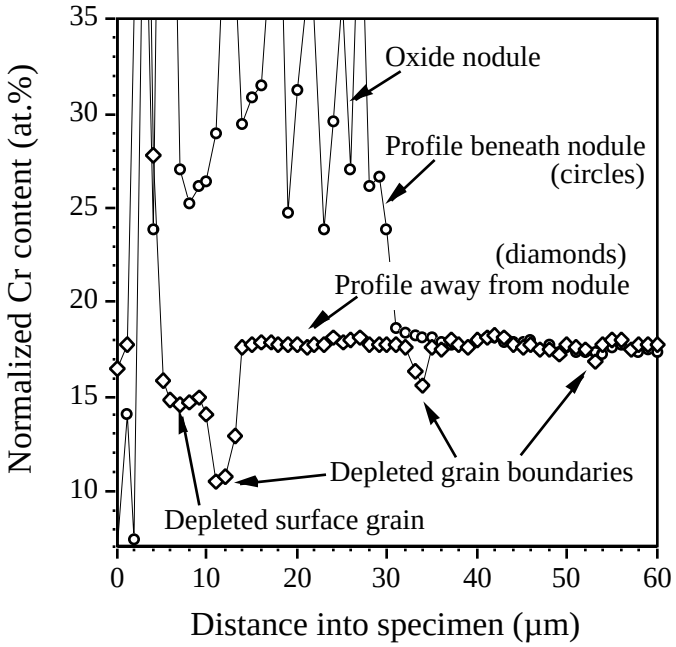

Figure 12. EPMA Cr profiles from two scans across the cross-section of Fe-16Cr-20Ni-2Mn+Si after 7,000h at 650°C in humid air. There is no depletion beneath the nodule. Without a nodule, the Cr is depleted in the grain adjacent to the surface and on alloy grain boundaries.

showed no Cr depletion in the underlying metal (Fig. 12). Before a nodule forms, the underlying metal is Cr-depleted. As the nodule grows, forming Fe-rich oxide, the adjacent substrate becomes enriched in Ni and appears to form a Ni-rich oxide below the nodule (Figs. 11c and 11d). This may explain the benefit of increasing the Ni content. With only 10wt.%Ni in type 347 stainless steel, the nodules may grow significantly larger before their growth is arrested by the formation of a Ni-rich or Cr-rich oxide. Information from higher-alloyed model materials may clarify the role of alloy composition in the formation and growth of nodules during AA.

DISCUSSION

Continued experimental work on the role of water vapor on oxidation behavior in exhaust gas environments is beginning to show a clearer picture of how austenitic steels are adversely affected by this environment. Initial work had shown that higher-alloyed steels were more resistant to AA[3]. Based on the current results, a higher Cr content is critical because Cr is mainly depleted from the near-surface region at 650° (e.g. Fig. 7) and 700°C. Also, because Cr depletion is concentrated at the specimen surface, increasing the specimen thickness does not assist in preventing AA.

Several hypotheses have been proposed about the role of Ni[8]. While none have been explicitly proven, it does appear that higher Ni contents may be beneficial in minimizing the growth of nodules during AA. Comparing the rates of Cr loss in the various commercial foils at 650° and 700°C (Table II), higher Ni contents did not reduce the consumption of Cr by oxidation/evaporation. However, in a model alloy with double the Ni content of type 347 stainless steel, Fe-16Cr-20Ni-2Mn, Ni-rich oxide was observed in nodules formed after 7,000h at 650°C (Fig. 11). Since NiO is slower growing than any of the iron

oxides[21], the formation of a Ni-rich oxide may slow the growth of the overlying nodule and more quickly allow the formation of an underlying Cr-rich oxide.

Previous work noted the role of alloy grain size on the onset of AA with finer-grained type 347 or ferritic steels being more resistant to AA than coarser-grained material of the same composition[9,22]. The benefit of a finer grain size is an increased Cr flux due to faster Cr transport on grain boundaries than in the bulk for both austenitic and ferritic steels[23]. The current results showing Cr depletion on alloy grain boundaries also reflects the faster grain boundary diffusion of Cr. At 650° and 700°C, slower Cr diffusion within alloy grains results in higher Cr contents at the center of grains, while the grain boundaries become depleted (Fig. 12). This selective depletion was not noted at 800°C[7,9] where there is less difference between bulk and grain boundary diffusion rates, and more uniform depletion profiles were observed. This difference in depletion behavior as a function of exposure temperature illustrates the problem with attempting to accelerate laboratory tests by increasing the test temperature. The most critical temperature range for stainless steels in recuperators is 600°-700°C and, even if the inlet temperature increases further, a significant portion of the recuperator will still operate in this temperature range.

While it was surprising to observe nodule formation and the onset of AA in higher-alloyed stainless steels like alloys 709 and 120, it is worth noting that the nodules formed in depleted regions near the surface and the underlying metal is essentially unaffected (e.g. Figs. 7 and 12). If nodule formation after 10,000h at 650° or 700°C is confined to the outer 5-10μm of material, there is still a high probability that ≈100μm foil will meet the 40,000h durability goal. The underlying material was essentially unaffected and a similar period of time should be required for the next layer of metal to be depleted and consumed. There appears to be a very low probability that any Fe-base alloy could operate for extended periods in this temperature range without some degradation due to Cr depletion and subsequent nodule formation. If the Fe-rich oxide remains adherent, this will eventually degrade heat transfer in the recuperator, a factor that should be considered in recuperator performance models. If the Fe-rich oxide spalls during service, there should be less effect on heat transfer, but the spall could collect and inhibit flow.

The quantification presented here of Cr depletion as a function of temperature (Table II) and time (Fig. 8) are specific values for the gas velocity (relatively low in this test compared to a recuperator) and water vapor content (relatively high) used in these experiments, and could vary significantly under different environmental conditions. In extrapolating these values to longer times, linear kinetics may be expected, because of the importance of evaporation during long-term exposures at 650°-700°C. However, the kinetics need to be confirmed at these temperatures, similar to the results at 800°C (Fig. 8). Future work also will examine Cr depletion in similar commercial alloys in the microturbine test facility at ORNL[24,25].

The standard deviations for the residual Cr results show the difficulty in making these measurements. Small changes in the measured remaining metal thickness will have a strong effect on the residual Cr measurement. Also, the non-uniform presence of oxide nodules in the profiles has a strong effect on the calculated Cr depletion values. Furthermore, the starting Cr content needs to be carefully verified. During thermo-mechanical processing to foil, some Cr depletion or other change in composition may occur, making composition measurements from the starting sheet stock (Table I) less applicable.

Finally, as cost is still an important issue for microturbine components, future work will examine the long-term viability of the leanest alloy compositions (Fe-20Cr-25Ni and Fe-20Cr-20Ni) for this application. Continued work is examining methods for improving the creep strength of these alloys, while maintaining the corrosion resistance. For a primary surface recuperator[10,13,19,26], creep strength is an important issue; however, for plate and fin recuperators[2], this is less of a priority.

SUMMARY

The completion of 10,000h laboratory oxidation exposures at 650°, 700° and 800°C of several candidate commercial alloys for advanced recuperators has yielded some important information about the role of water vapor in this environment. Even with high levels of Cr and Ni, Fe-base alloys exhibited the onset of Fe-rich nodule formation, due to Cr depletion near the alloy substrate surface, particularly at alloy grain boundaries. At 650°-700°C, only the outer 10-20μm of material is affected, with no change in composition for the inner foil material. This localized attack is likely due to the relatively slow diffusion of Cr in this temperature range. Results on commercial alloys and model alloys indicate that higher Cr and/or Ni contents confer more resistance to this form of attack. Quantification of the residual Cr content in the commercial alloy foils showed similar amounts of Cr consumption for all of the materials at 650° and 700°C, illustrating the benefit of a higher starting Cr content. These observations will need to be taken into account for development of a lifetime model.

ACKNOWLEDGMENTS

The author would like to thank J. D. Vought, G. W. Garner, K. S. Reeves, H. Longmire and L. R. Walker at ORNL for assistance with the experimental work and P. J. Maziasz, I. G. Wright and P. F. Tortorelli for comments on the manuscript. This research was sponsored by the U.S. Department of Energy, Distributed Energy Program under contract DE-AC05-00OR22725 with UT-Battelle, LLC.

REFERENCES

1. McDonald, C. F., 2003, "Recuperator Considerations for Future Higher Efficiency Microturbines," Applied Thermal Engineering, **23**, pp.1463-87.
2. Kesseli, J., Wolf, T., Nash, J. and Freedman, S., 2003, "Micro, Industrial, and Advanced Gas Turbines Employing Recuperators," ASME Paper #GT2003-38938, presented at the International Gas Turbine & Aeroengine Congress & Exhibition, Atlanta, GA, June 2-5, 2003.
3. Pint, B. A. and Rakowski, J. M., 2000, "Effect of Water Vapor on the Oxidation Resistance of Stainless Steels," NACE Paper 00-259, Houston, TX, presented at NACE Corrosion 2000, Orlando, FL, March 2000.
4. Rakowski, J. M. and Pint, B. A., 2000, "Observations on the Effect of Water Vapor on the Elevated Temperature Oxidation of Austenitic Stainless Steel Foil," NACE Paper 00-517, Houston, TX, presented at NACE Corrosion 2000, Orlando, FL, March 2000.
5. Asteman, H., Svensson, J.-E., Norell, M. and Johansson, L.-G., 2000, "Influence of Water Vapor and Flow Rate on the High-Temperature Oxidation of 304L; Effect of Chromium Oxide

Hydroxide Evaporation," Oxidation of Metals, **54**, pp.11-26.5.
6. Rakowski, J. M., 2001, "The Oxidation of Austenitic Stainless Steel Foils in Humidified Air," ASME Paper 2001-GT-360, presented at the International Gas Turbine & Aeroengine Congress & Exhibition, Amsterdam, Netherlands, June 3-6, 2002.
7. Pint, B. A. and More, K. L., 2004, "Stainless Steels with Improved Oxidation Resistance for Recuperators," ASME Paper #GT2004-53627, presented at the International Gas Turbine & Aeroengine Congress & Exhibition, Vienna, Austria, June 14-17, 2004.
8. Peraldi, R. and Pint, B. A., 2004, "Effect of Cr and Ni Contents on the Oxidation Behavior of Ferritic and Austenitic Model Alloys in Air With Water Vapor," Oxidation of Metals, **61**, pp.463-83.
9. Pint, B. A., Peraldi, R. and Maziasz, P. J., 2004, "The Use of Model Alloys to Develop Corrosion-Resistant Stainless Steels," Materials Science Forum, **461-464**, pp.799-806.
10. Stambler, I., 2004, "Mercury 50 rated at 4600kW and 38.5% efficiency with 5ppm NO_x," Gas Turbine World, Feb-Mar 2004, pp.12-16.
11. Watts, J. H., 1999, "Microturbines: A New Class of Gas Turbine Engine," Global Gas Turbine News, **39**(1), pp.4-8.
12. Kikuchi, M., Sakakibara, M., Otoguro, Y., Mimura, H., Araki, S. and Fujita, T., 1985, "An Austenitic Heat Resisting Steel Tube Developed for Advanced Fossil-Fired Steam Plants," in High Temperature Alloys, Their Exploitable Potential, J. B. Marriott, M. Merz, J. Nihoul and J. Ward Eds., Elsevier, London, pp.267-76.
13. Rakowski, J. M., Stinner, C. P., Lipschutz, M. and Montague, J. P., 2004, "The Use and Performance of Oxidation and Creep-Resistant Stainless Steels in an Exhaust Gas Primary Surface Recuperator Application," ASME Paper #GT2004-53917, presented at the International Gas Turbine & Aeroengine Congress & Exhibition, Vienna, Austria, June 14-17, 2004.
14. Pint, B. A. and Maziasz, P. J., 2005, "Development of High Creep Strength and Corrosion-Resistant Stainless steels," NACE Paper 05-449, Houston, TX, presented at NACE Corrosion 2005, Houston, TX, April 2005.
15. Office of Energy Efficiency and Renewable Energy, Office of Power Technologies, March 2000, "Advanced Microturbine Systems Program, Plan for Fiscal Years 2000 Through 2006," U. S. Department of Energy, Washington, DC.
16. Pieraggi, B., 1987, "Calculations of Parabolic Reaction Rate Constants," Oxidation of Metals, **27**, pp.177-85.
17. Marasco, A. L. and Young, D. J., 1991, "The Oxidation of Iron-Chromium-Manganese Alloys at 900°C," Oxidation of Metals, **36**, pp.157-74.
18. Quadakkers, W. J., Malkow, T., Piron-Abellan, J., Flesch, U., Shemet, V. and Singheiser, L., 2000, "Suitability of Ferritic Steels for Application as Construction Materials for SOFC Interconnects," Proc. 4th Eur. Solid Oxide Fuel Cell Forum, Vol. 2, A. J. McEvoy Ed., Elsevier, Amsterdam,pp.827-36.
19. Maziasz, P. J., Swindeman, R. W., Shingledecker, J. P., More, K. L., Pint, B. A., Lara-Curzio, E. and Evans, N. D., 2003, "Improving High-Temperature Performance of Austenitic Stainless Steels for Advanced Microturbine Recuperators," in Parsons 2003, Engineering Issues in Turbine Machinery, Power Plant and Renewables, Maney, London, pp.1057-73.
20. Maziasz, P. J., Shingledecker, J. P., Pint, B. A., Evans, N. D., Yamamoto, Y., More, K. L. and Lara-Curzio, E., 2005, "Overview of Creep Strength and Oxidation of Heat-Resistant Alloy Sheets and Foils for Compact Heat-Exchangers," ASME Paper #GT2005-68927, presented at the International Gas Turbine & Aeroengine Congress & Exhibition, Reno-Tahoe, NV, June 6-9, 2005.
21. Kofstad, P., 1988, High Temperature Corrosion, Elsevier Applied Science Publishing, London.
22. Pint, B. A. and Peraldi, R., 2003, "Factors Affecting Corrosion Resistance of Recuperator Alloys," ASME Paper #GT2003-38692, presented at the International Gas Turbine & Aeroengine Congress & Exhibition, Atlanta, GA, June 2-5, 2003.
23. Tökei, Zs., Hennesen, K., Viefhaus, H. and Grabke, H. J., 2000, "Diffusion of Chromium in Ferritic and Austenitic 9-20 Wt.% Chromium Steels," Materials Science Technology, **16**, pp.1129-1138.
24. Lara-Curzio, E., Maziasz, P. J., Pint, B. A., Stewart, M., Hamrin D., Lipovich, N. and DeMore, D., 2002, "Test Facility for Screening and Evaluating Candidate Materials for Advanced Microturbine Recuperators," ASME Paper #2002-GT-30581, presented at the International Gas Turbine & Aeroengine Congress & Exhibition, Amsterdam, Netherlands, June 3-6, 2002.
25. Lara-Curzio, E., Trejo, R., More, K. L., Maziasz, P. J. and Pint, B. A., 2005, "Evaluation and Characterization of Iron- and Nickel-Based Alloys for Microturbine Recuperators," ASME Paper #GT2005-68630, presented at the International Gas Turbine & Aeroengine Congress & Exhibition, Reno-Tahoe, NV, June 6-9, 2005.
26. Maziasz, P. J. and Swindeman, R. W., 2003, "Selecting and Developing Advanced Alloys for Creep-Resistance for Microturbine Recuperator Applications," Journal of Engineering for Gas Turbines and Power, **125**, pp.51-58.